Modeling Thermo-electrochemistry, Capacity Degradation, and Mechanics with SEI Layer

Prof. Ann Marie Sastry, PI

Project ID: ES082

Arthur F. Thurnau Professor, Mechanical, Biomedical and Materials Science and Engineering
University of Michigan
Ann Arbor, MI 48109-2125

CONTRIBUTORS: **Dr. Jonghyun Park, Dr. Jeong Hun Seo, Dr. Amit Gupta, Prof. Wei Shyy, Mr. Min Zhu**

2011 DOE Annual Merit Review Meeting
Arlington | May 11, 2011

This presentation does not contain any proprietary or confidential information

Advanced Materials Systems Laboratory

Departments of Mechanical, Biomedical and Materials Science and Engineering

acknowledgements

sponsor

DOE

Sastry group members

Dr. Joseph Gallegos
Dr. Sangmin Lee
Mr. Yoon Koo Lee
Dr. Greg Less
Mr. Sang Woo Han
Mr. Dong Hoon Song
Mr. Ho Sop Shin

leverage

General Motors
Oak Ridge National Laboratory

timeline and budget

timeline

- project start date: Jan. 2010
- project end date: Apr. 2011
- percent complete: 90%

budget

- total project funding
  - DOE share: $ 320 K
- funding received in FY10
  - $ 320 K
- funding for FY11
  - N/A

barriers

BARRIERS: short lithium battery lifetimes—capacity degradation, closely related to composition of electrode, particle aggregates and dissolution of particles; closely related to SEI layer formation on electrodes

electrode configuration (e.g., composition)

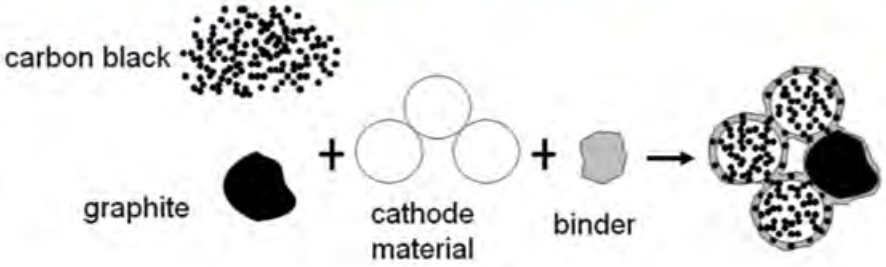

dissolution of active material particles

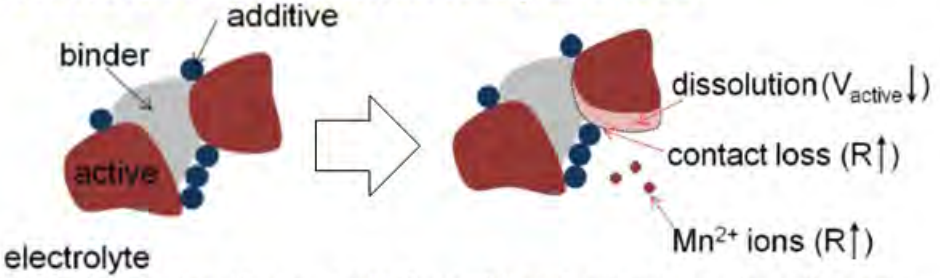

[1] J. Park, J.H. Seo, G. Plett, W. Lu and A.M. Sastry, "Numerical simulation of the effect of the dissolution of LiMn2O4 particles on Li-ion battery performance," *Electrochem. Solid-State Lett.*, v. 14 (2), pp. A14-A18, 2011

particle aggregates (active material & additives)

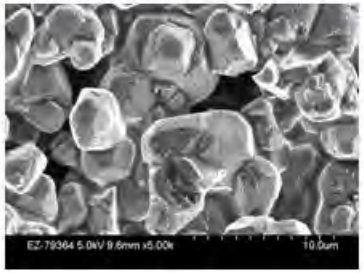

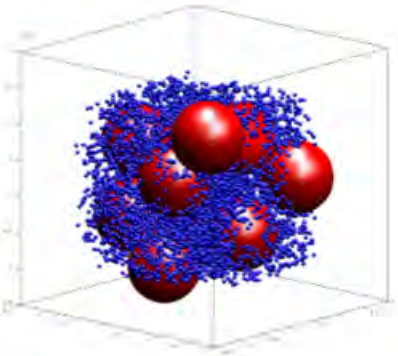

SEI layer formation

[2]

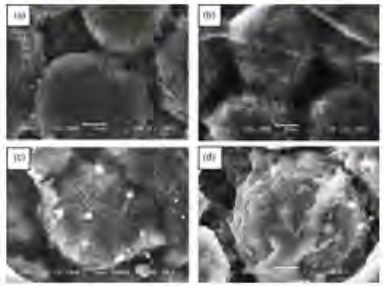

[3]

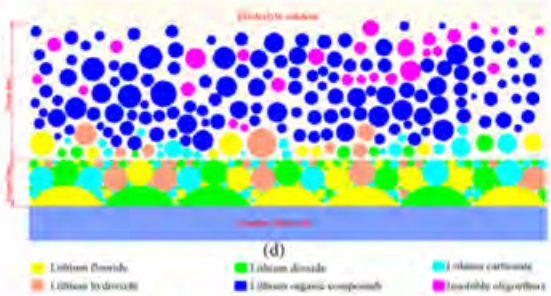

[2] P.L. Moss, G. Au, E.J. Plichta and J.P. Zheng, "Investigation of solid electrolyte interfacial layer development during continuous cycling using ac impedance spectra and micro-structural analysis," *Journal of Power Sources*, v. 189 (1), 2009

[3] J. Yana, B.-J. Xia, Y.-C. Su, X.-Z. Zhou, J. Zhang, X.-G. Zhang, "Phenomenologically modeling the formation and evolution of the solid electrolyte interface on the graphite electrode for lithium-ion batteries," *Electrochimica Acta*, v. 53, pp.7069-7078, 2008

overview / lab efforts

A • M • S • L

atomic/molecular:
understand chemistry

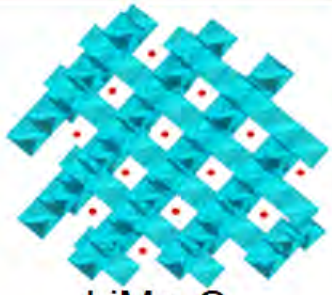

$LiMn_2O_4$

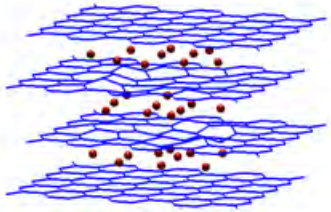

graphite

materials synthesis

DoE: particle multiphysics simulations (08); aggregation (09)

particle-scale:
understand physics

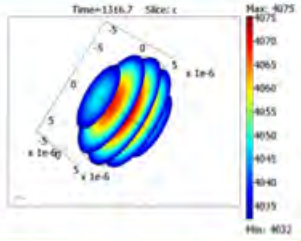

DoE/ORNL (08-09)

thin film

particle

GM (08-09)

GM: ongoing

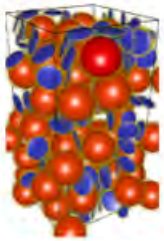

micro-scale:
understand mechanics

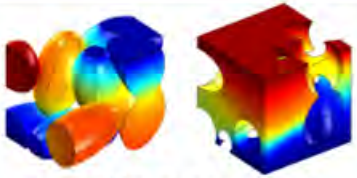

reaction current

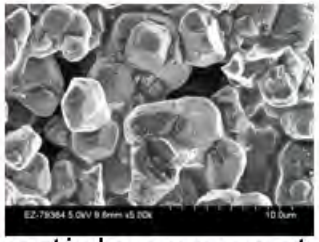

particle aggregates

GM: ongoing

performance testing

macro-scale:
battery optimization

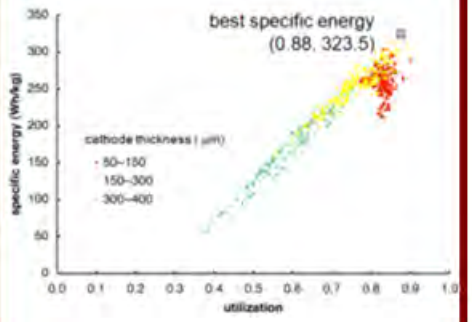

purpose of work

OBJECTIVES:

Determine battery performance for high-power systems via multiscale FE modeling considering self-assembly, and the effect in turn on cathode dissolution as the main effect in capacity degradation. Investigate SEI layer formation mechanism. Validate SEI layer formation model through *ex situ* experimental techniques.

MILESTONES:

(a) implement multiscale modeling with self-assembly and dissolution (Mar. 11) (implemented)
(b) implement modeling and simulation for multiple nucleation formation (May 11)
(c) characterize microstructure, chemical elements of SEI layers, and impedance change due to SEI layers (Aug. 11)

dissolution of active particles: FY10

objectives

- derive volume fraction changes in electrodes due to dissolution and extend the porous electrode theory to correlate dissolution with capacity fade in Li-ion batteries
- map the nature of the effects of dissolution on the capacity decrease during cycling with different conditions, including temperature and voltage range

approach

- calculate volume loss due to dissolution using shrinking unreacted-core model
- simulate 1D thermal-electrochemical model for battery performance
- study capacity fade and resistance change by changing temperature, voltage range, and cycle number

finding/results

- a quantitative relationship between the volume fraction change due to dissolution and capacity fade
- material loss of active particles results in decreased effective transport properties in the solid phase, which in turn results in a reduction in electrochemical reaction rate, reducing capacity

publications

- Park, J., Seo, J.H., Plett, G., Lu, W. and Sastry, A.M., "Numerical simulation of the effect of the dissolution of $LiMn_2O_4$ particles on Li-ion battery performance", *Electrochemical and Solid-State Letters*, v. 14 (2), pp. A14-A18, 2011

dissolution of active particles: FY10

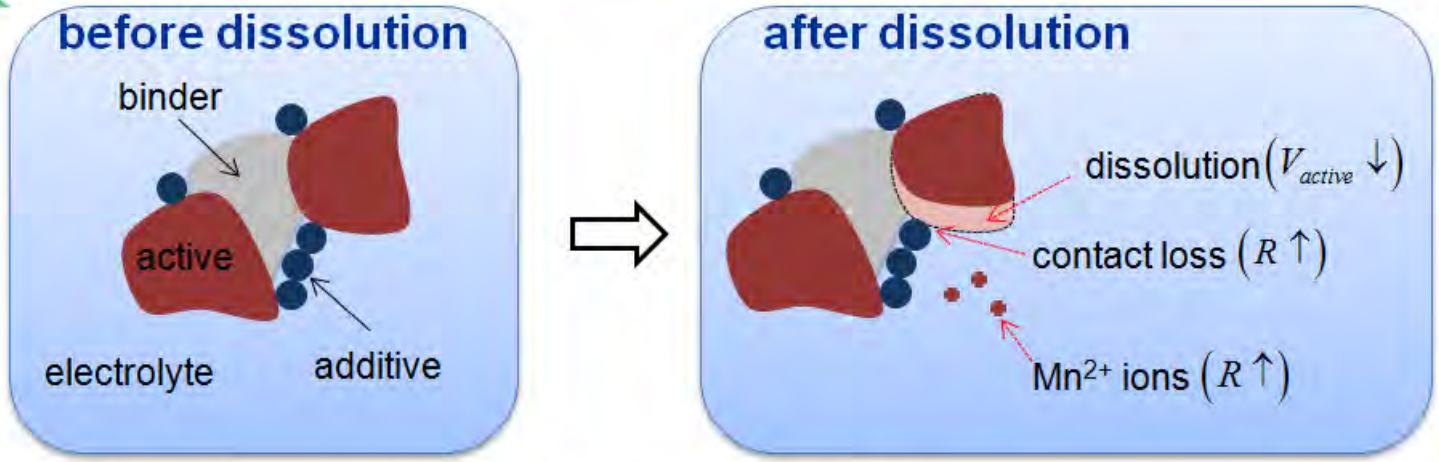

three main factors determining dissolution rate

- particle size: contact surface area
- temperature: reaction rate
- operating voltage: phase transition

main dissolution effects on battery performance

- active material loss leads to direct capacity loss
- loss decreases the effective transport properties, resulting in a reduction of the electrochemical reaction rate, reducing capacity
- contact resistance increases due to the intimate contact loss between active and conductive particles
- the dissolved Mn^{2+} ions transported, deposited on the anode side; deplete the anode by the reduction of Mn

dissolution of active particles: FY10

AAS measurement

- dissolution ratio and reaction time [1, 2]
- $\left[1-(1-X_a)^{1/3}\right]=kt$

  X_a : the dissolution reaction

volume loss estimation

- $\frac{M_d^{3+}}{M_i^{3+}}=\frac{X_a}{1+X_a}, M_d^{4+}=\frac{1}{2}M_d^{3+}$
- $V=V_0\left(1-\frac{0.304}{2}\frac{X_a}{X_a+4}\right)$

  i: initial, *d*: dissolved molar mass

thermal-electrochemical model

- galvanostatic charge/discharge simulations with a limited voltage range

properties

battery system	
anode	graphite (100 μm)
cathode	manganese oxide (183 μm)
electrolyte	1M $LiPF_6$ in EC:DMC

dissolving rate	
particle	19.9 μm in diameter (cathode) [1]
E_a^*	72.84 kJ/mol [1]
K_0^*	3.41×10^5 s^{-1} [1]
ω^{**}	2.8 times [3]

* k is expressed by Arrhenius representation $k=k_0\exp(-E_a/RT)$

** elevated reaction rate above 4.1 V and below 3.1 V

[1] C.-H. Lu and S.-W. Lin, *J. Mater. Res.*, **17**, 1476 (2002)
[2] O. Levenspiel, *Chemical Reaction Engineering*, John Wiley & Sons, New York (1972)
[3] Y. Xia, Y. Zhou, and M. Yoshio, *J. Electrochem. Soc.*, **144**, 2593 1997

dissolution of active particles: FY10

discharge voltage profile

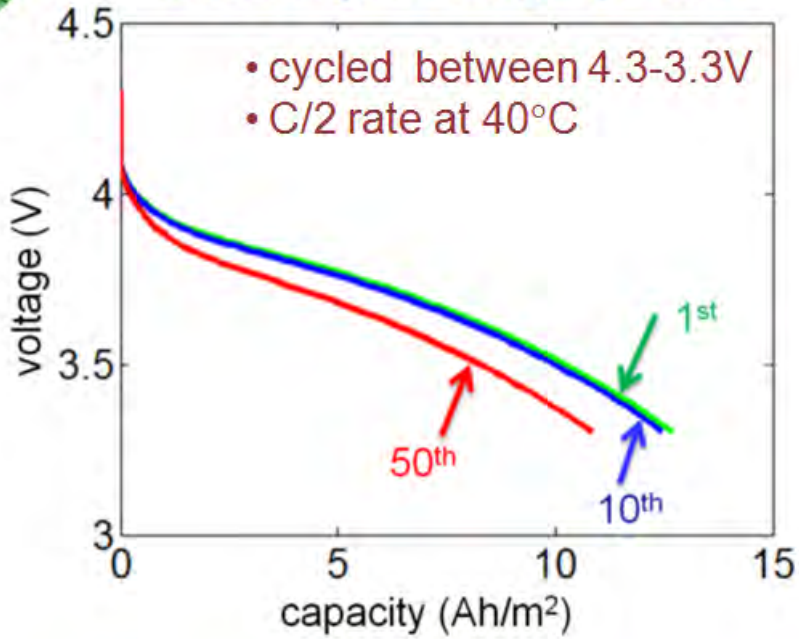

resistance change

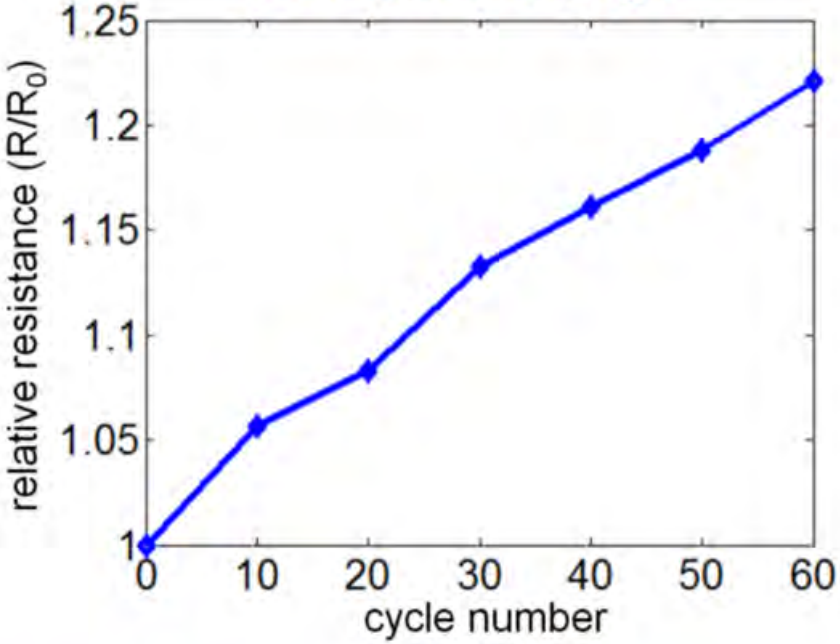

- after 50 cycles, the capacity decreases by 15% due to dissolution of the active particles
- the active material loss causes a delay in the reaction rate for insertion and deinsertion at the solid and electrolyte phase boundary, which results in an increase in resistance; the increase in resistance will cause a high polarization, resulting in apparent capacity losses

dissolution of active particles: FY10

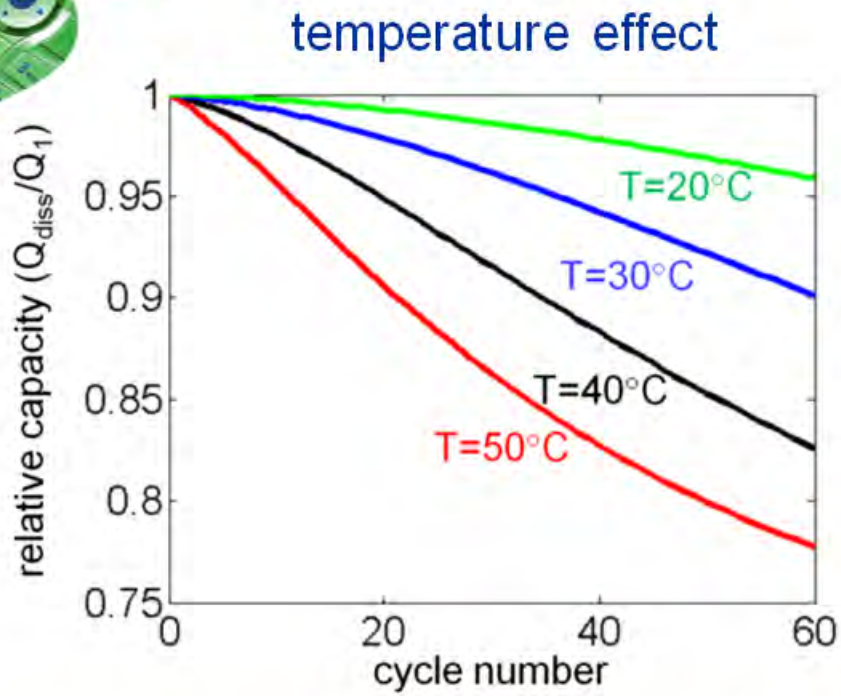

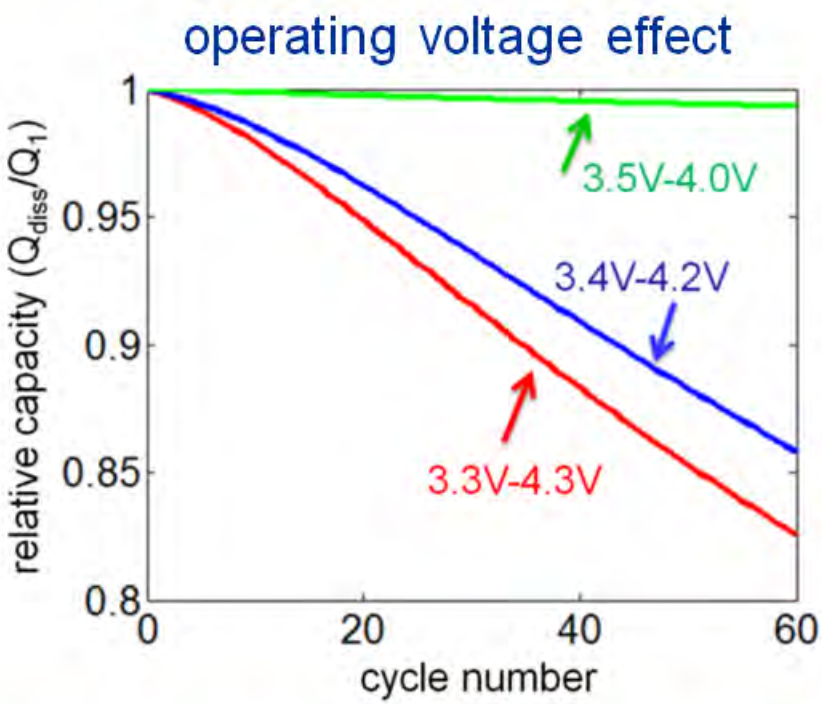

- due to a higher temperature and a wider range of voltages, greater dissolution of cathode particles was shown to result in a severe capacity fade using the models derived here
- the capacity fade increases by a factor of 5 when the temperature increases by 30 C after 60 cycles, and the cycling with a wider voltage range results in a 25% increase in the capacity fade after 60 cycles

heat generation model [1,2]

- heat generation due to side reactions can be significant when thermal runaway starts
- heat of mixing O(10^{-14}) is negligible compared to resistive heat O(10^{-12}) and entropic heat O(10^{-12}) at particle scale [2]

symbol	meaning
T	temperature
$\dot{Q}_g$	heat generation rate
I	current
U	open circuit potential
V	potential
ΔH_k^{avg}	enthalpy of reaction for chemical reaction k
r_k	rate of reaction k
$\bar{H}_{ij}$	partial molar enthalpy of species i in phase j
$\bar{H}_{ij}^{avg}$	volume-averaged partial molar enthalpy
c_{ij}	concentration of species i in phase j

$$\dot{Q}_g = I_1 \cdot \nabla V_1 + I_2 \cdot \nabla V_2 + J\left(V_1 - V_2 - U + T\frac{\partial U}{\partial T}\right) + \sum_k \Delta H_k^{avg} r_k + \int \sum_j \sum_i \left(\bar{H}_{ij} - \bar{H}_{ij}^{avg}\right)\frac{\partial c_{ij}}{\partial t} dv$$

resistive heating

reaction heating

entropic heat (reversible, due to entropy change)

heat change due to side reactions

heat of mixing (due to concentration gradient)

not considered

[1] Thomas, K.E. and Newman, J., "Thermal modeling of porous insertion electrodes," *J. Electrochem. Soc.*, v. 150, pp. A176-A192, 2003
[2] Zhang, X.C., Sastry, A.M., and W. Shyy, "Intercalation-induced stress and heat generation within single lithium-ion battery cathode," *J. Electrochem. Soc.*, v. 155(7), pp.A542-A552.

thermo-electrochemistry: FY10

microscopic scale

3-D electrode microstructure

liquid phase (electrolyte)

solid phase (active material)

both phase

interphase

$$\frac{\partial c_2}{\partial t} = \nabla \cdot \left(D_2 \nabla c_2 \right)$$

$$\nabla \cdot \left[\kappa \nabla V_2 + \kappa_D \nabla \left(\ln c_2 \right) \right] = 0$$

$$\frac{\partial c_1}{\partial t} = \nabla \cdot \left(D_1 \nabla c_1 \right)$$

$$\nabla \cdot \mathbf{i}_1 = \nabla \cdot \left(\sigma \nabla V_1 \right) = 0$$

$$\rho c_p \frac{\partial T_k}{\partial t} = \nabla \cdot \left(\lambda_k \nabla T_k \right) + i_k \cdot \nabla V_k$$

Butler-Volmer equation

$$J = \frac{i_n}{F} = i_0 \left\{ \exp\left[\frac{(1-\beta)F}{RT} \eta \right] - \exp\left[-\frac{\beta F}{RT} \eta \right] \right\}$$

Arrhenius equation

$$\phi = \phi_{ref} \exp\left[\frac{E_{act,\phi}}{R} \left(\frac{1}{T_{ref}} - \frac{1}{T} \right) \right]$$

volume averaging

macroscopic scale

1-D Li-ion cell

anode | separator | cathode

$$\frac{\partial \overline{c_2}}{\partial t} = \nabla \cdot \left(D_2^{\text{eff}} \nabla \overline{c_2} \right) + J_{c_2}$$

$$\nabla \cdot \left[\kappa^{\text{eff}} \nabla \overline{V_2} + \varepsilon_2 \kappa_D^{\text{eff}} \nabla \left(\ln \overline{c_2} \right) \right] + J_{V_2} = 0$$

$$\frac{\partial \overline{c_1}}{\partial t} = \nabla \cdot \left(D_1^{\text{eff}} \nabla \overline{c_1} \right) + J_{c_1}$$

$$\sigma^{\text{eff}} \nabla \overline{V_1} + J_{V_1} = 0$$

$$\rho^{\text{eff}} c_p^{\text{eff}} \frac{\partial \overline{T}}{\partial t} = \nabla \cdot \left(\lambda^{\text{eff}} \nabla \overline{T} \right) + \overline{Q}$$

closure terms (D^{eff}, κ^{eff}, λ^{eff}, J, Q):
highly depend on the detailed microstructure

- effective material properties
- volumetric reaction current density
- heat generation

thermo-electrochemistry: FY10

closure terms: reaction current density & heat generation at solid-electrolyte interphase (SEI)

Li-ion flux (isothermal)

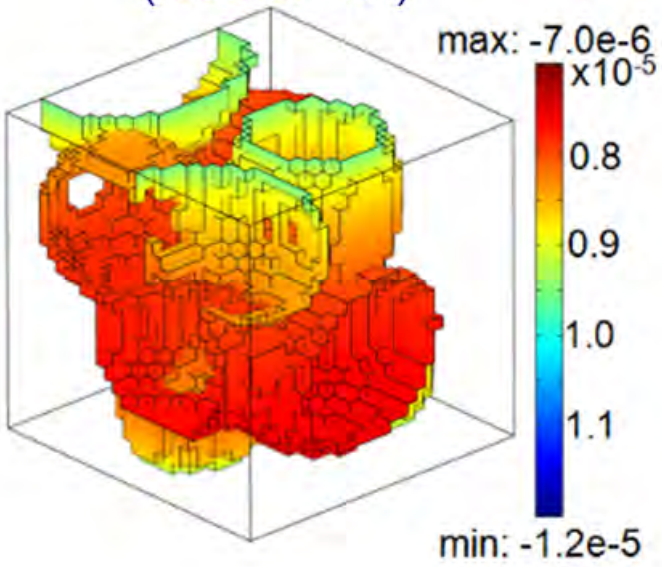

Li-ion flux (non-isothermal)

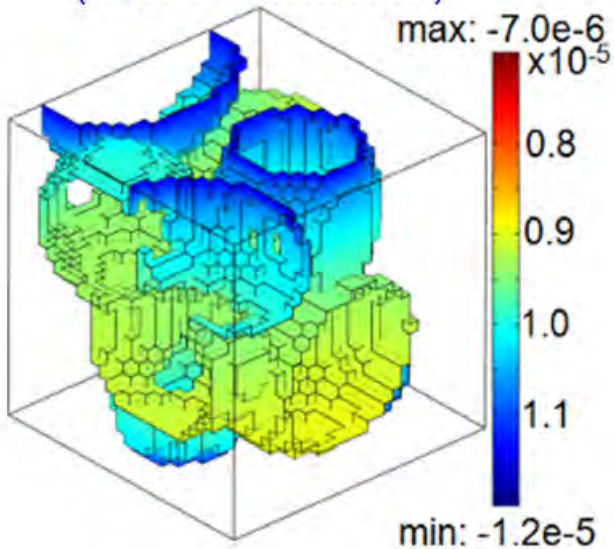

heat generation (non-isothermal)

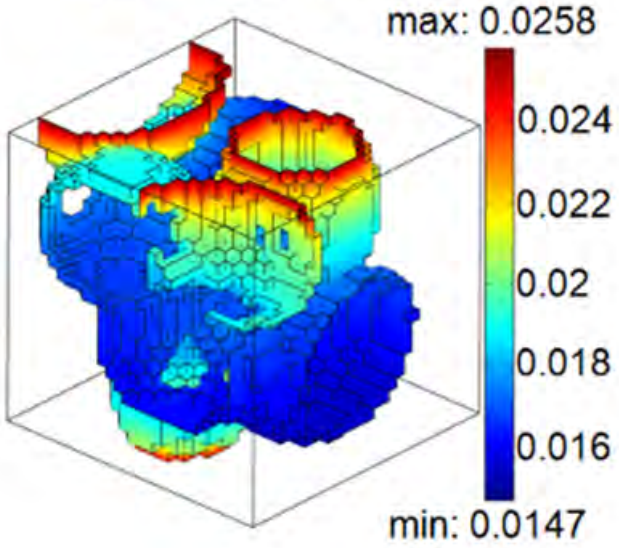

non-isothermal model with temperature-dependent reaction and transport properties gives higher Li-ion flux at the solid-electrolyte interphase

closure terms comparison

temporal variations of reaction current density and heat generation from the pseudo-2D thermo-electrochemical model and 3D microscopic model

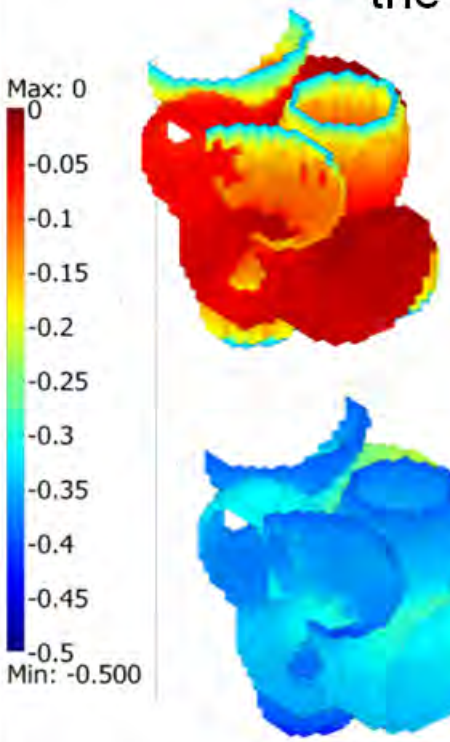

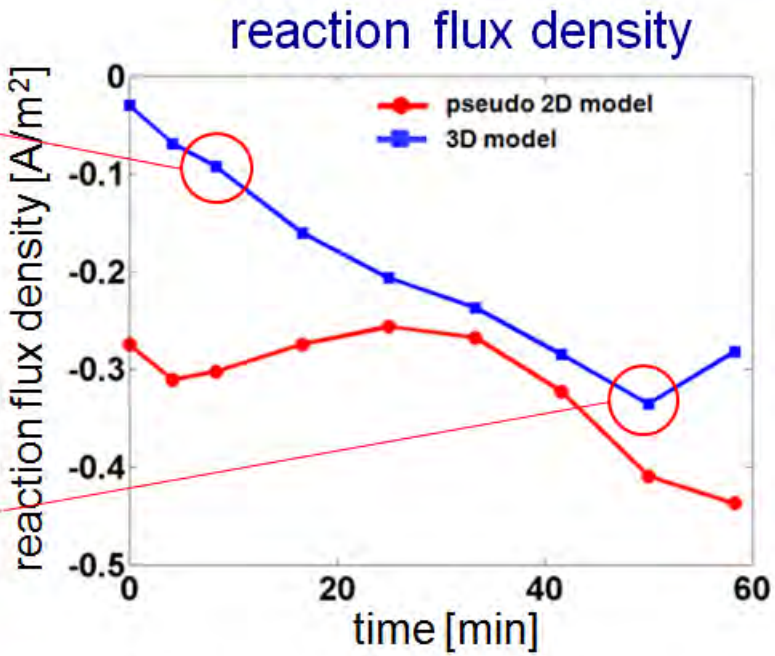

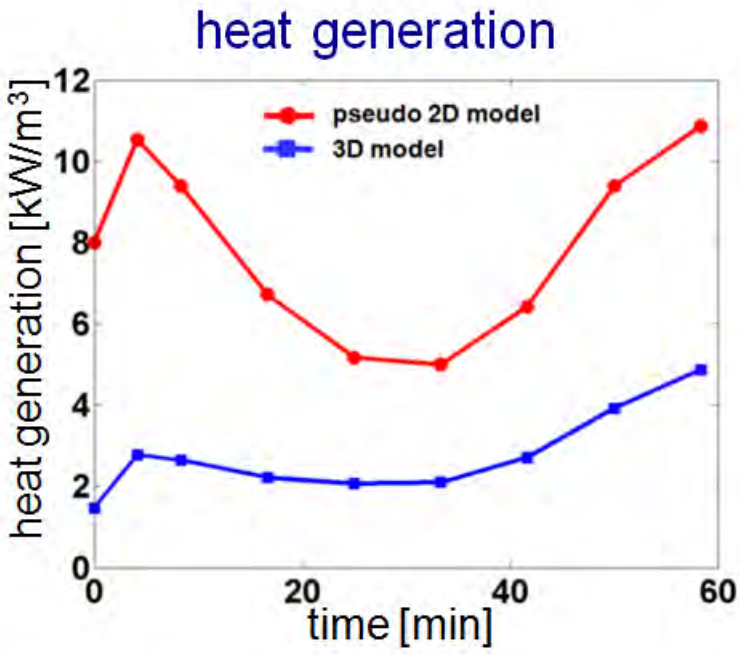

3-D microscopic modeling of particle microstructure reveals distribution of local state variables (e.g., Li-ion concentration and electric potentials in solid and electrolyte phases)

multiscale modeling: surrogate-based scale bridging

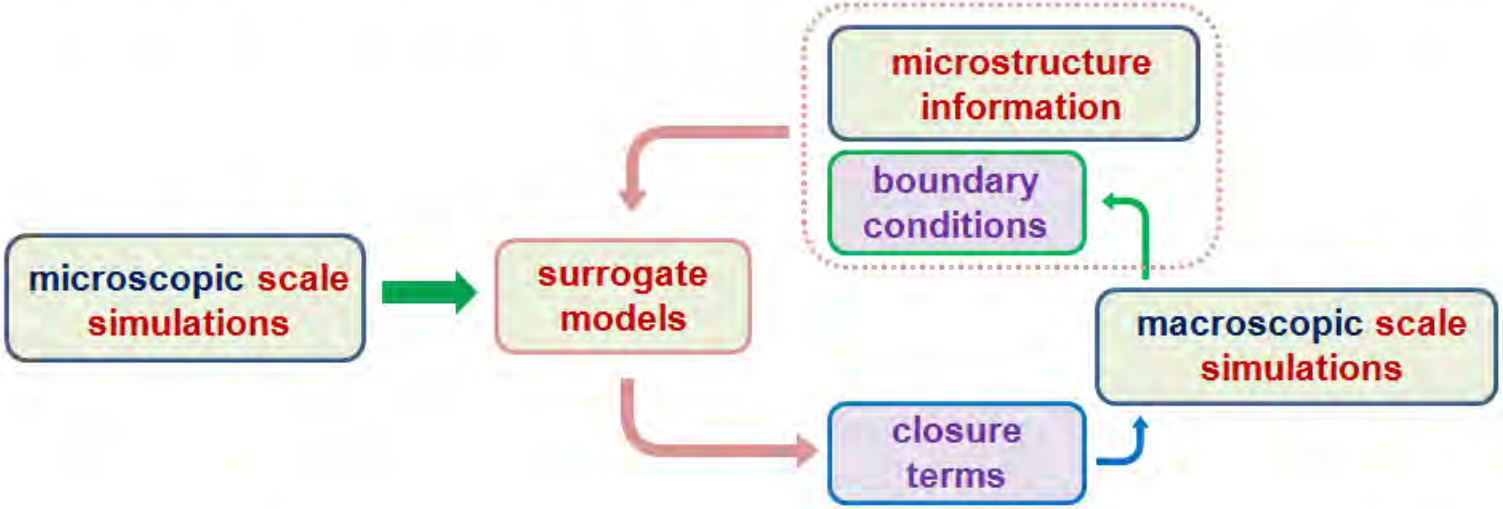

- surrogate modeling of closure terms (reaction current density and heat generation) in thermo-electrochemistry: key steps include design of experiment on state variables (e.g., Li-ion concentration and electric potentials), running numerical simulations, construction of surrogate models, validation
- global sensitivity analysis: constructed surrogate models are used to quantify quantification of the variation of the closure terms caused by state variables

surrogate modeling of closure terms:
reaction current density and heat generation

- **design variables & their range**

Variables	Symbol	Range	Unit
Li ion concentration (solid)	$\tilde{c}_1$	0.15 ~ 0.6	1
Li ion concentration gradient (solid)	$\tilde{c}_{1,z}$	-8000 ~ 1000	1/m
Electric potential (solid)	V_1	2.6 ~ 4.1	V
Electric potential gradient (solid)	$V_{1,z}$	-80 ~ 0	V/m
Li ion concentration (liquid)	c_2	800 ~ 2000	mol/m^3
Li ion concentration gradient (liquid)	$c_{2,z}$	$-1.7x10^7$ ~ $6x10^5$	mol/m^4
Electric potential (liquid)	V_2	-1.5 ~ 0	V
Electric potential gradient (liquid)	$V_{2,z}$	-1300 ~ 0	V/m
Temperature	T	290 ~ 340	K
Temperature gradient	T_z	-1.5 ~ 0	K/m

- **design space range**
  based on pseudo 2D solutions up to 3C discharge rates

- **constraint of design space**
  bounds for surface overpotentials to avoid numerical issues from exponential term in Butler-Volmer equation

$$-0.1 \le V_1 - V_2 - U(\tilde{c}_1) \le 0$$

- **design of experiments**
  face centered composite design (FCCD) and Latin hypercube sampling (LHS) were used to generate a set of simulation points as design of experiments (DOE).

global sensitivity analysis

reaction flux density

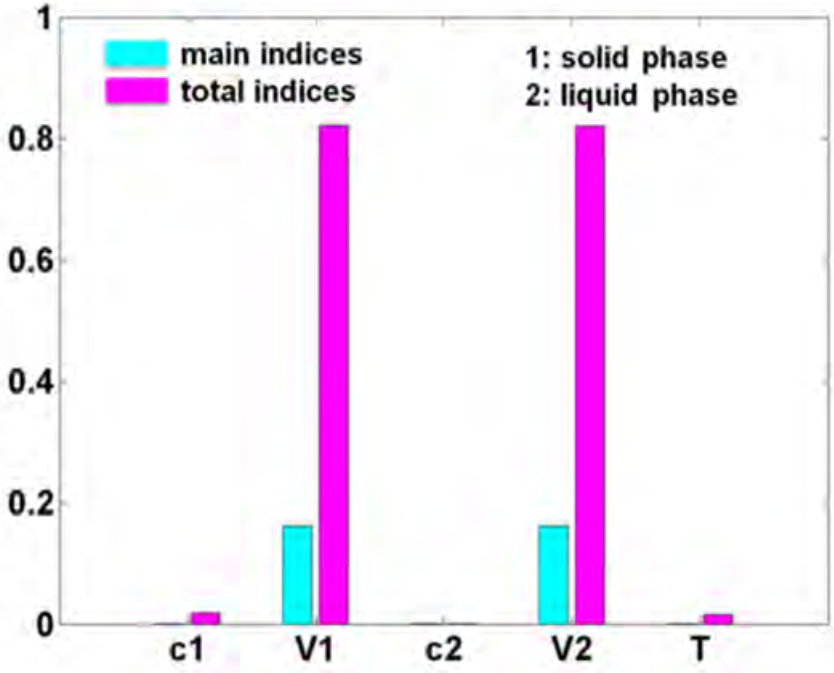

heat generation

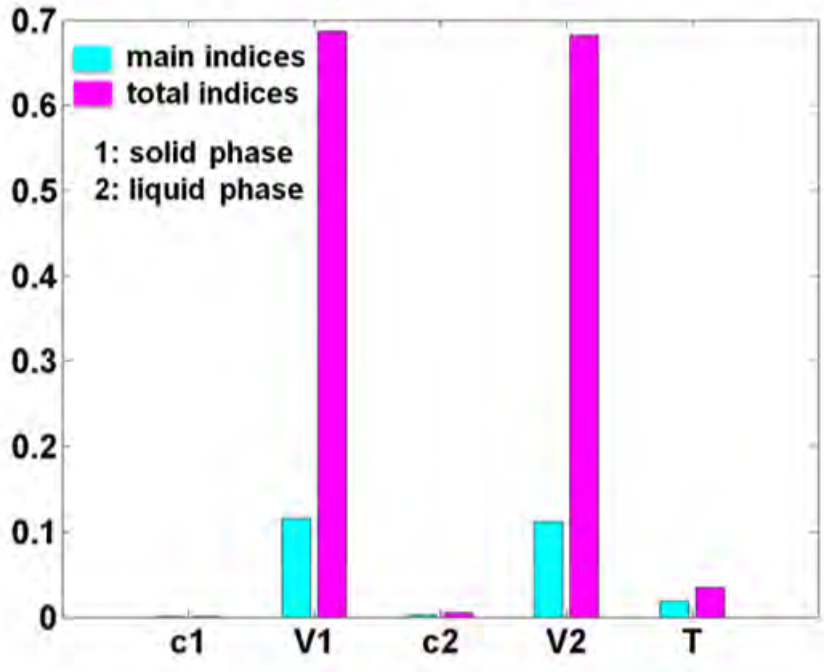

electric potentials in solid and electrolyte phase dominates in surrogate models of reaction flux density and heat generation

SEI formation modeling: FY10

experimental observation

two distinct layers [1-4]

- a thin compact polycrystalline layer enriched with inorganic species (electrode side)
- a thick, porous, and amorphous layer enriched with organic compound (2nd layer)
- confirmed by XPS, SEM, AFM measurements

nucleation and growth process [5]

- highly ordered phyrolytic graphite (HOPG) surface remains clean and smooth (higher than 2V, Fig 1,3); exhibit a few isolated solid islands on edge (below 1.6V); an abundance of solid clusters (below 0.8V, Fig 2,4)
- SEI is non-uniform and composed of secondary solid micrograins

Fig. 1

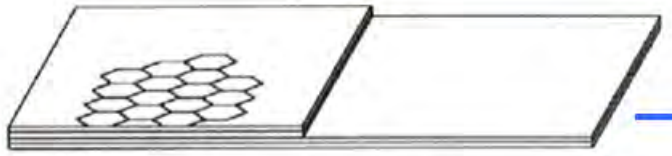

Fig. 2

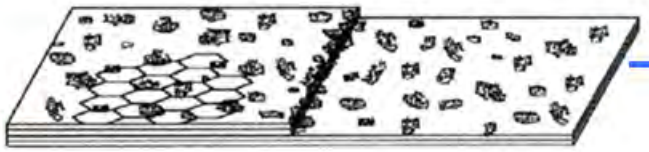

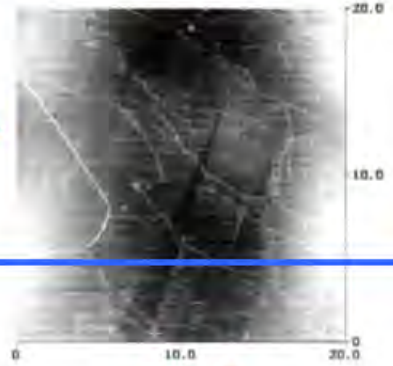

Fig. 3

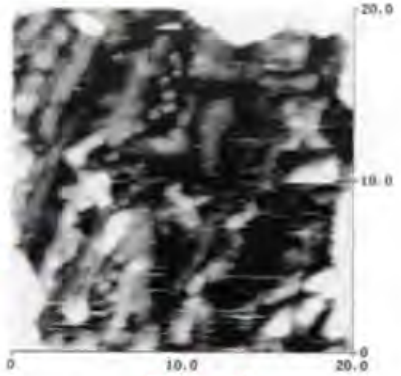

Fig. 4

[1] J. Yan *et al*, Electrochimica Acta 53, 7069 (2008)
[2] D. Bar-Tow *et al*, J. Electrochem. Soc. 146, 824 (1999)
[3] A.M. Andersson *et al*, J. Power Sources, 119-121, 522 (2003)
[4] D. Aurbach, *et al*, J. Electrochem. Soc. 143, 3525 (1996)
[5] A.C. Chu *et al*, J. Electrochem. Soc, 144, 4161 (1997)

SEI formation modeling: FY10

SEI formation

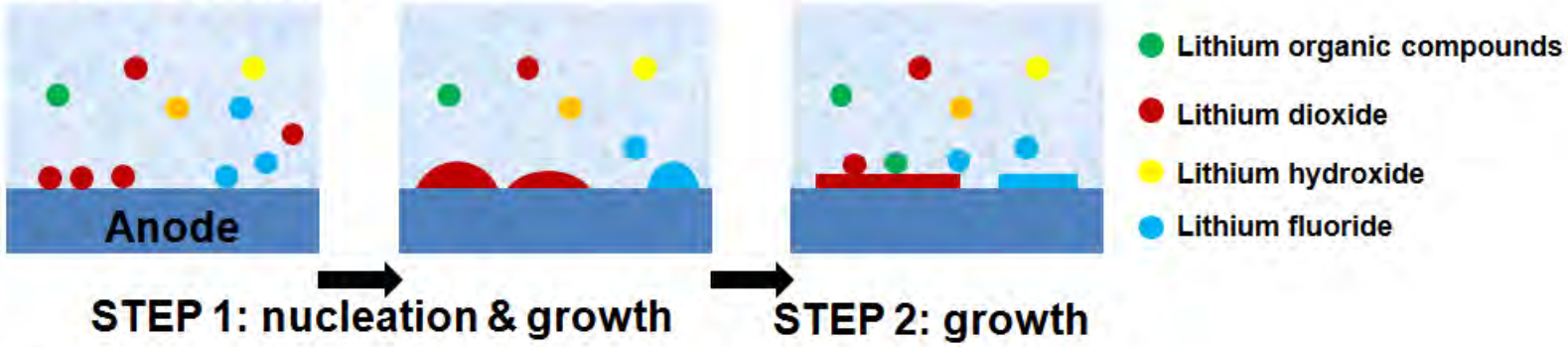

nucleation [1,2]

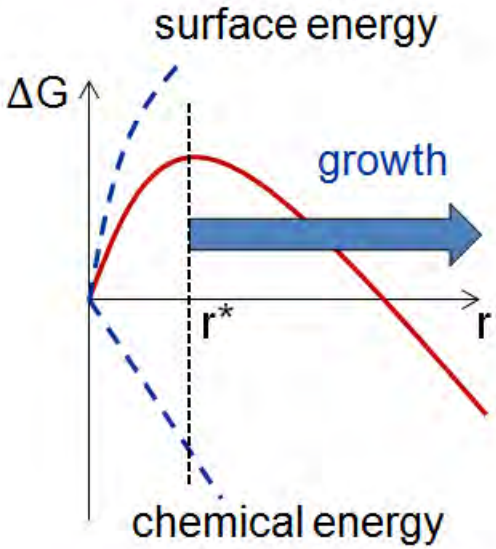

- competition between chemical energy and surface energy
- some nuclei cannot grow, dissolve into the parent phase
- r<r*, surface energy dominates (shrinks)

→

- if a nucleation is formed, the final geometry affects the surface roughness, therefore the new-formed layer is affected by the pre-formed layers
- how to determine the geometry of the nucleation? microstructure evolution problem

[1] J. Yan et al, Electrochimica Acta, 53, 7069 (2008)
[2] J.W. Christian, The Theory of Transformations in Metals and Alloys, Oxford (2002)

SEI formation modeling: FY10

phase field method approach

$$G = \int_\Omega \left(f(c) + \frac{1}{2} h(\nabla c)^2 \right) dS + \int_{\partial\Omega} [\sigma_{SA} + (\sigma_{SE} - \sigma_{SA})\rho(c)] dl$$

chemical energy — interfacial energy — surface energy

(S: solid, A: anode, E: electrolyte)

extend (plan)

roughness change (affect new layer)

single particle nucleation

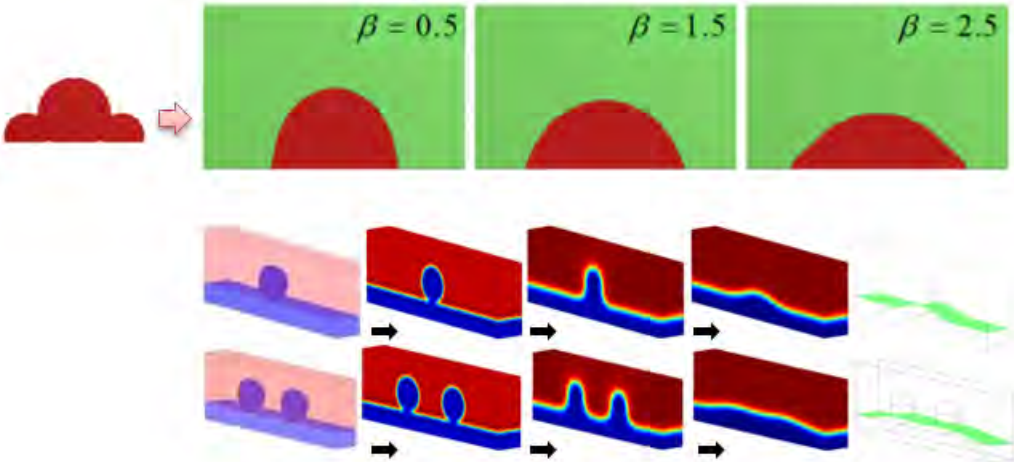

$$\beta = L_c(\sigma_{SE} - \sigma_{SA}) / h$$

hetero-nucleation

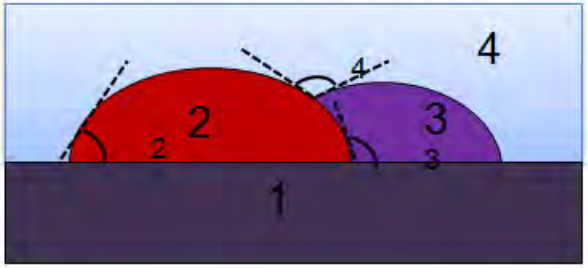

local equilibrium angles

$$\sigma_{14} - \sigma_{24}\cos\theta_2 - \sigma_{12} = 0$$

$$\sigma_{13} + \sigma_{12} - \sigma_{23}\cos\theta_3 = 0$$

$$\sigma_{13} - \sigma_{24} - \sigma_{34}\cos\theta_4 = 0$$

self-assembly in cathodes: FY10

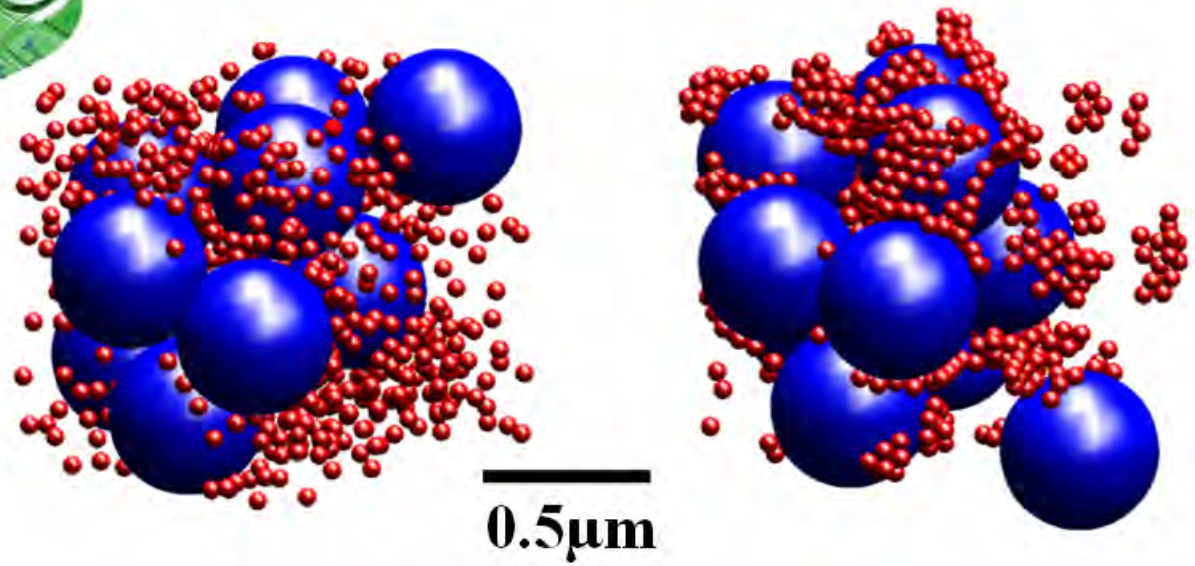

initial configuration final configuration

T=308K
active material particle size 0.5µm and 1.0µm
AM:CB mass ratio 4%:92%
volume fraction of AM and CB: 50%
unit cell size: 4.7 times of the AM radius

active material (AM)

carbon black (CB)

- all AM particles are aggregated into a single cluster and percolate the simulation domain
- local aggregates of CB particles are observed
- CB particles are also observed to connect to the percolated AM clusters

self-assembly in cathodes: FY10

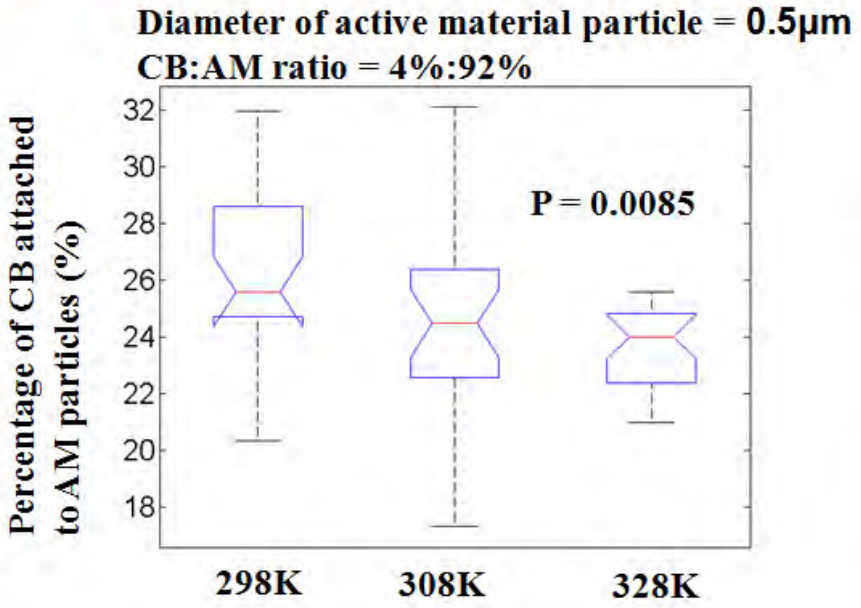

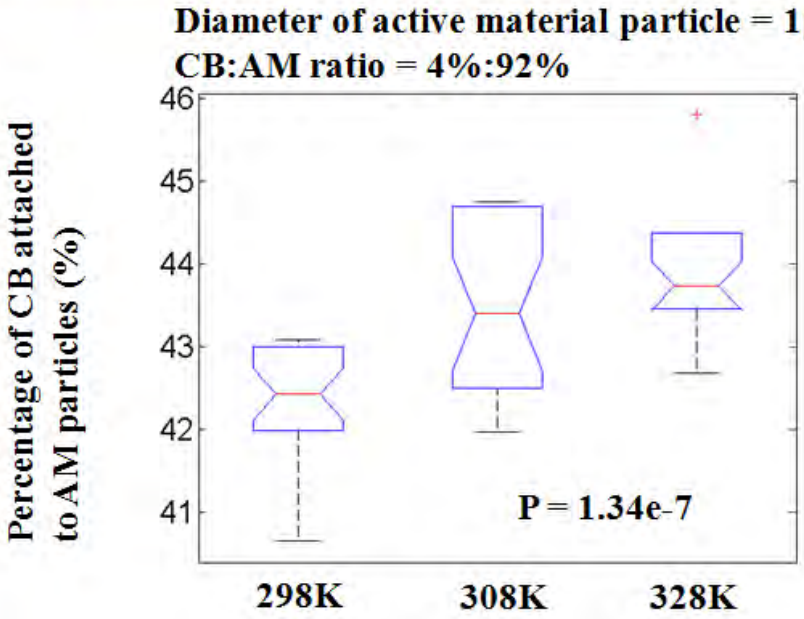

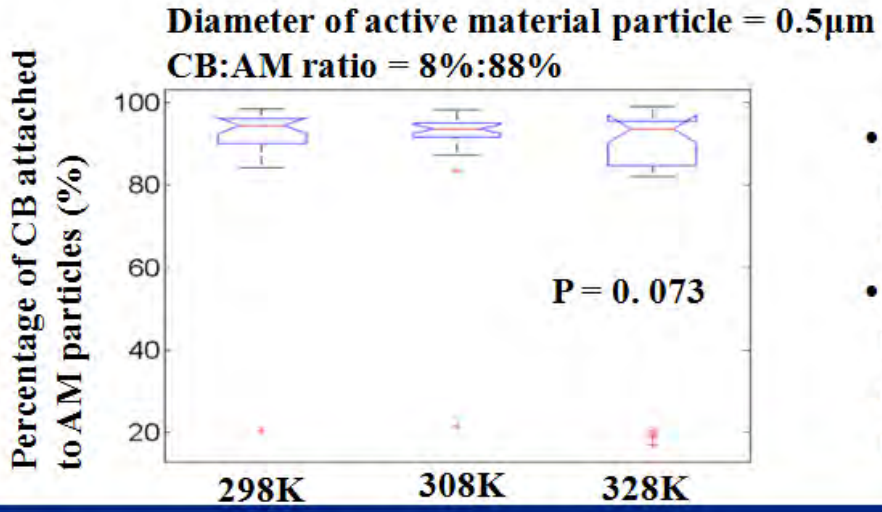

- a larger AM particle size and larger CB/AM mass ratios each contribute positively to the percentage of CB attachment
- with increasing temperature this percentage increases in cases where AM particles have a diameter of 1μm but decreases for AM particles whose diameter is 0.5μm

accomplishments and status

- **Fundamental:** The changes in effective transport properties and electrochemical kinetics due to dissolution were incorporated into a thermo-electrochemical model to study capacity fade due to dissolution. **Practical:** this provides a quantitative and direct relationship between the volume fraction change due to dissolution and capacity fade.
- **Fundamental:** A multiscale thermo-electrochemistry was applied to include non-isothermal effects of the electrode microstructure on battery scale modeling. **Practical:** the constructed surrogate models give good predictions of the closure terms (i.e., reaction current density and heat generation) and reveal the significance of state variables (i.e., Li-ion concentrations and electric potentials).
- **Fundamental:** Brownian dynamics was employed to simulate the self-assembly of particles in Li-ion battery cathodes. **Practical:** the self-assembled structures were characterized by the percentage attachment of carbon black to active material clusters. The effect of temperature, mass ratio and particle size was investigated.
- **Fundamental:** The formation and evolution of the SEI layer was modeled, which had been observed via several experiments. **Practical:** The model explains the possible mechanism for the origin of the two distinct layers comprising the SEI layer.

future work

- continue to refine numerical models based on findings from simulated performance and experiments; parameters to be investigated include multi-phase particle structures, resistances in SEI films, and temperature dependence of material transport properties and film resistance

- investigate SEI formation in composite electrode microstructures and its effect on battery kinetics and thermo-electrochemical performance; both experimental and numerical tools will be employed

- continue to explore progressive capacity degradation in composite multi-phase electrodes in the context of multiple scales and multiphysics coupling electrochemical kinetics and thermal effects

summary

- numerical modeling of dissolution shows a quantitative relationship between the volume fraction change due to active material dissolution and capacity fade
- material loss of active particles results in decreased effective transport properties in the solid phase, which in turn results in a reduction in electrochemical reaction rate, reducing capacity
- 3-D microscopic modeling of particle microstructure reveals local distribution of state variables (Li-ion concentration and electric potentials) in thermal-electrochemical model
- global sensitivity analysis of surrogate models shows that electric potentials in solid and electrolyte phase dominates in the closure terms (reaction flux density and heat generation)
- self assembly simulation shows that a larger AM particle size and larger CB/AM mass ratios each contribute positively to the percentage of CB attachment
- with increasing temperature this percentage increases in cases where AM particles have a diameter of 1μm but decreases for AM particles whose diameter is 0.5μm